Chalmers Publication Library

(article starts on next page)

OTA Testing in Multipath of Antennas and Wireless Devices with MIMO and OFDM

Per-Simon Kildal, *Fellow, IEEE*, Charlie Orlenius, *Member, IEEE,* Jan Carlsson, *Member IEEE*

Abstract—: **New Over-The-Air (OTA) measurement technology is wanted for quantitative testing of modern wireless devices for use in multipath. We show that the reverberation chamber emulates a rich isotropic multipath (RIMP), making it an extreme reference environment for testing of wireless devices. This complements thereby testing in anechoic chambers representing the opposite extreme reference environment: pure Line-of-Sight (LOS).**

Antenna diversity gain was defined for RIMP environments based on improved fading performance. The present paper finds this RIMP-diversity gain also valid as a metric of the cumulative improvement of the 1% worst users randomly distributed in the RIMP environment.

The paper argues that LOS in modern wireless systems is random due to randomness of the orientations of the users and their devices. This leads to the definition of cumulative LOS-diversity gain of the 1% worst users in random LOS. This is generally not equal to the RIMP-diversity gain.

The paper overviews the research on reverberation chambers for testing of wireless devices in RIMP environments. Finally, it presents a simple theory that can accurately model measured throughput for LTE system with OFDM and MIMO, the effects of which can clearly be seen and depend on the controllable time delay spread in the chamber.

Index Terms— **antenna measurements, MIMO, multipath, OTA measurements, Rayleigh fading, reverberation chamber**

I. INTRODUCTION

A NTENNA measurements are traditionally done in anechoic chambers emulating free space, because free space is a good reference environment for antenna locations on rooftops and masts, with Line-Of-Sight (LOS) to the opposite side of the communication link. However, modern small antennas on wireless devices are not located on masts and rooftops, and they are exposed to multipath and resulting large signal variations referred to as fading, and often there is not LOS at all. The present paper describes a completely different reference environment than the free space one, i.e. a rich isotropic multipath (RIMP) environment; suitable for Over-The-Air (OTA) testing of small antennas and wireless devices intended for use in multipath. The isotropic multipath environment is characterized by a uniform distribution of the Angles-Of-Arrival (AoA) over all directions in space, so that the evaluated performance becomes statistically independent of the orientation of the wireless device.

Modern wireless devices have and will be provided with small multi-port antennas mitigating the negative effects of fading by using adaptive spatial modulation in the forms of antenna diversity and MIMO (Multiple Input Multiple Output) technology. Therefore, there is a need for well defined test environments with time-varying fading, such as the statistical RIMP with arbitrary time-variation of phase, amplitude and polarizations of the incident waves, in order to test the quality of the fading-adapted coding and receiver.

This paper will summarize how real-life multipath environments are characterized in time, frequency and spatial domains, and in addition how these characteristics must be understood for arbitrary locations, and in particular arbitrary orientations of the users and their wireless devices (Section III). This user-distributed arbitrariness causes the wireless device to experience any LOS as a random LOS, in terms of its AoA being randomly distributed among many users' and devices' orientations. The introduction of a random LOS is of course not new, see e.g. [1], [2], neither including statistics of the user [3]. However, the new content of the present approach is that we consider the random LOS to be a 3D-random LOS (Section IV) and take the consequence of this user-distributed 3D-randomness to accept the isotropic 3D environment as a representative reference environment for statistical evaluations of performance of antennas and wireless devices with small antennas. We also acknowledge this by interpreting in a new way the RIMP-diversity gains defined in [4, 5]. They were previously interpreted as fading improvements of a single moving user (device), whereas now we interpret them as representing the cumulative gains of the 1% worst stationary users in RIMP. This also leads to introduction of a new representative 3D-random LOS-diversity gain (Section V); complementing the RIMP-diversity gain [6].

The paper is relevant for the developments of standards for characterization of base stations, terminals and other devices for wireless communication systems, and in particular new wireless systems such as IEEE 802.11n (WiFi), LTE and WiMAX. These systems have the capability of mitigating fading by using diversity in both spatial and frequency domains, by means of MIMO and OFDM (Orthogonal Frequency-Division Multiplexing) technology, respectively.

The reverberation chamber has been used for three decades for EMC measurements [7], and if it is well designed and large enough, it represents an ideal RIMP environment [4]. Its performance is based on well accepted theories [8, 9], and it has during the last decade shown its ability to accurately measure efficiency, diversity gain and MIMO capacity [4, 10] of passive antenna systems; as well as radiated power, receiver sensitivity [11], diversity gain and throughput data rate [12] of active mobile devices. The early basic works [4, 10] have later been updated with new algorithms for predicting diversity gain more accurately [13, 14], as well as new understanding of how to improve measurement accuracy [15], and how to control the time and frequency domain characteristics of the reverberation chamber, i.e. delay spread and coherence bandwidth, respectively [16], and fading speed and Doppler spread. The present paper will summarize the developments that have been done since [4, 10] were published (Section VI) and in particular those related to throughput measurements (Section VII) and modeling (Section VIII). It will also be shown how throughput curves can be used to determine performance of the 1% worst users (Section IX),

II. OVERVIEW OF OTA MEASUREMENT APPROACHES

Traditionally, antennas were always located on masts or roof-tops in order to make sure that there was LOS between the transmitting and receiving antennas, and, there were certain requirements to the height of the mast or roof in order to avoid destructive interference from ground reflections. Then, the characterizing quantity of each antenna was its realized gain and directivity in the direction of the opposing antenna, and in addition there could be requirements on sidelobes in the radiation pattern in order to ensure that the received signal is not degraded due to reflections from nearby objects, or due to interference by disturbing signals from other antenna systems. Reflecting objects in the environment are unavoidable, but the antennas for LOS systems were still and only characterized in free-space-type environment such as anechoic chambers, with presence neither of ground nor reflecting objects. And, all requirements have traditionally been specified relative to measurements in this pure-LOS environment, although in practice the performance will depend on e.g. how high above ground an antenna is mounted. Such additional constraints have been developed and reported and are used together with anechoic test results to ensure good performance in real-life situations. Together with such constraints, the anechoic chamber is a well-accepted reference environment for testing of antennas and antenna systems for use in LOS environments. The further developments of the anechoic chamber have been towards more advanced chambers in order to reduce size, i.e. compact ranges and spherical near-field ranges, or measurement time, i.e. multi-probe systems, or both [17].

Modern mobile communication systems work also when the devices are located in multipath environments of different kinds with severe fading, such as those appearing in urban and indoor environments. In such environments the radiation pattern and directivity play no role anymore, or at least a very minor role compared to LOS systems, because many interfering waves with unknown angles of arrival (AoA) and arbitrary amplitude and phase, contribute to the resulting statistically fluctuating received signal voltage, i.e. the fading radio channel. Looking at individual antenna ports and RIMP environments, the characterizing quality metric is the classical total radiation efficiency. This accounts for contributions due to several factors: mismatch, imperfect lossy materials of the antenna, losses in the materials of the device itself, and losses in nearby objects such as the user's hand or head [4]. It is important to note that this total radiation efficiency is the same as that defined for an antenna in a traditional pure-LOS environment, which can be measured in anechoic chambers.

Future wireless devices will to higher degree make use of multi-port MIMO antennas to mitigate the problems of fading dips in which the device may not work; requiring also testing of MIMO and diversity algorithms for combining the different channels received on each port to new channels with reduced fading. The latter is for a moving user characterized by a diversity gain [4] at the 1% level of the Cumulative Distribution Function (CDF) of the received signal voltage. Here, we will equivalently discuss it as a cumulative diversity gain for the 1% worst users, i.e. the 1% users with the worst performance in terms of received signal level, as already mentioned in the introduction.

The fading multipath environment can be emulated in several ways. The multi-probe anechoic chamber such as the one described in [17] can emulate it, but it is not very suitable in terms of size and cost. Therefore, many multi-probe systems under study make use of a simple planar (2D) ring of probes rather than a 3D distribution of them [18]. Another reason is that most of the existing theoretical propagation models have been developed for 2D AoA distributions only (i.e. AoA in horizontal plane), because this is easier to deal with analytically than 3D environments. Still, in spite of all the ongoing developments of the anechoic chamber for characterization of antennas in multipath, we were not able to find more scientifically reviewed journal articles than [18].

The reverberation chamber can emulate multipath by using only one transmitting probe antenna, in contrast to anechoic chambers requiring many probes. This simplicity of the reverberation chamber makes it much more cost-effective.

The mobile devices themselves have till now mainly been characterized for the transmitting case, whereas the appearance of smart phones in the market has given the receiving function much more attention. This is characterized by the input signal level at which a specified bit error rate (BER) is achieved.

The new wideband mobile communication systems have bandwidths that are much larger than the coherence bandwidth of most environments, causing frequency selective fading. The frequency fading is mitigated by frequency diversity, e.g. as implemented in OFDM technology. Therefore, the testing of wireless devices of such systems must be done subject to frequency selective fading, and it has been verified that such related tests of throughput data rate can be done in reverberation chambers [12] (Section VIII).

It should be mentioned that the frequency selective fading also can be generated in anechoic chambers, but then it requires the use of special and expensive electronic instruments called fading emulators, and even several such instruments may be needed to get frequency selective fading at all probes, i.e. for all incident wave directions. This will make the anechoic multi-probe fading emulators in [18, 19] even more complex and expensive compared to reverberation chambers.

III. CHARACTERIZATION OF THE WIRELESS CHANNEL IN TIME, FREQUENCY AND SPACE DOMAINS

Note that we here include both the transmitting and receiving antennas in the definition of the channel, because we cannot have any wireless channel without having both a transmitting antenna to excite it and a receiving antenna to detect it. Therefore, the wireless channel performance is to large extent determined by the antennas themselves, and the channel performance cannot be separated from the antenna performance.

The undisturbed *pure-LOS radio channel* is characterized entirely in terms of the realized gains of the transmitting and receiving antennas, and the space attenuation. The realized gain is a deterministic spatial antenna characteristic that is invariant with time, and the bandwidth of the LOS channel is determined entirely by the bandwidths of the two antennas. On the other hand, the spatial characteristics of the *RIMP channels* are statistical with an average received power determined by the radiation efficiencies of the transmitting and receiving antennas and not their realized gains, which will be discussed in more detail below. In addition, the RIMP channel has both statistical frequency and time domain characteristics that influence the performance of the communication system (Table 1).

Table 1. Parameters characterizing multipath environment [20]

Physical mechanism causing phenomena	Observed characterizing parameters (Fourier transform pairs) in time and frequency domain	
Fading speed	Coherence time	Doppler spread
Spatial depth	RMS delay spread	Coherence bandwidth

A. Fading speed and spatial depth

The fading varies with time due to movements of the transmitting device (base station), receiving device (terminal), or scattering objects in the environment. If the speeds of these movements are constant, we will still observe a corresponding frequency spectrum, because the different incoming waves (rays) have different angles of arrival relative to the movements, and therefore cause different Doppler shift. Thus, the width of this frequency spectrum is referred to as the Doppler spread. This corresponds to statistical coherence time in the time domain; see Table 1.

The incoming ray fields may have been reflected and scattered many times on their way between the transmitting and receiving sides of the channel. Therefore, they arrive with different time delays. The length of this delay is determined by

the spatial depth of the locations of the scattering objects in the environment, but also by their density, because among very dense scatterers the waves will attenuate faster and not propagate too far, so the scattering volume will be smaller. This phenomenon is characterized by an RMS (root mean square) delay spread in the time domain, corresponding to a coherence bandwidth in the frequency domain; see Table 1.

If we want to generate multipath in an anechoic chamber, we need an electronic channel emulator (an expensive instrument) on the transmitting side of the measurement set-up in order to emulate different time delay spreads and coherence bandwidths. The reverberation chamber, on the other hand, has inherent coherence bandwidths and time delay spreads that are similar to those appearing in real-life multipath environments [16], so for most multipath scenarios the electronic channel emulator is not needed when using reverberation chambers.

B. Frequency-flat and frequency-selective fading

When dealing with wireless systems there are two very different fading scenarios present: frequency-flat and frequency-selective fading. The frequency-flat fading refers to the fact that the signal bandwidth is so small that there is no effect of the fading within the signal bandwidth. This appears if the coherence bandwidth of the channel is much larger than the signal bandwidth, which was the case in the first wireless communication systems. The name frequency-flat fading relates to the fact that the autocorrelation function of the wireless channel in frequency domain is flat (i.e. constant) over the signal bandwidth.

However, with the present and future wideband WiFi, LTE and WiMAX systems the bandwidths are so large that the frequency autocorrelation function will be narrower than the signal bandwidth, so that the signal will experience distortions of the modulation and associated irreducible bit errors. This is referred to as frequency-selective fading. The OFDM system is built up to mitigate frequency selective fading by using many separate subcarriers that each is narrowband enough to experience frequency-flat fading.

C. Directional spatial domain

When wireless devices are exposed to Rayleigh fading, the received complex voltage (i.e. having both an amplitude and a phase) has a complex Gaussian distribution. The Rayleigh term is associated with the magnitude of the complex voltage that is observed to be Rayleigh distributed. The primary *complex Gaussian distribution* of the voltage makes the nature of the fading very fundamental, because the fading becomes a result of the central limit theory in statistics for independent complex variables [9]. We can also state that the complex Gaussian distribution is a result of the principle of maximum entropy. Thus, when the number of independent incoming waves increases, the distribution of the received voltage magnitudes (taken over many users or over time when one user moves) approaches the Rayleigh distribution.

The polarization of the incident waves in the multipath environment is of interest. We choose here to characterize this

in terms of *polarization balance*, instead of the more common term cross-polarization, because the latter really does not make sense in rich multipath. We have no co- or cross-polarization in a rich multipath. The polarization is random, but there could be an imbalance between the average power levels in the vertical and horizontal components of it, depending on the polarization of the base station. If we do not know the polarization of the base station, there will naturally be balance in *expected* polarization, i.e. the average received power in vertical and horizontal polarizations will be equal.

IV. TWO EXTREME REFERENCE ENVIRONMENTS: FREE SPACE AND RICH ISOTROPIC MULTIPATH (RIMP)

Table 2 describes the spatial characteristics of different types of wave propagation environments and the related antenna quality factors. We can observe how the anechoic chamber and the reverberation chamber represent the two extreme environments *"pure-LOS" and "RIMP"*, respectively. The common advantage of these two environments is that each one of them can be associated with one unique parameter that describes the primary performance of a single-port antenna, being the realized gain for the pure-LOS (if AoA is known, i.e. the deterministic case in frame 3.1 in the table) and the total radiation efficiency for the RIMP (frame 3.4). For the other real-life environments in between free space and RIMP, it is not normally possible to determine such a unique characterizing parameter of the antenna. Still, several of the real-life environments may appear statistically like being isotropic; when evaluated over a distribution of many different users at random locations and orientations, and with random orientations of their wireless device, which we will discuss in detail below.

Table 2. Characteristics of different environments and their antenna and multi-port antenna quality factors for devices with 3D-random orientations, i.e. arbitrary orientation in both the azimuth (2D) and elevation planes. Total radiation efficiency includes both mismatch and dissipation losses; for the multi-port case it is the total embedded element efficiencies at each port. Realized antenna gain = Directivity * Total radiation efficiency

Environment:	1. Ideal free space (pure-LOS)	2. Real-life free space	3. Real-life multipath	4. Rich isotropic multipath (RIMP)
1. Possible measurement method:	Anechoic chamber (AC)	AC & guidelines	RC & calculation of LOS-diversity gain	Reverb. chamber (RC)
2. Characteristics:	LOS with deterministic dual polarizations	LOS & some multipath e.g. ground reflections	Polarization imbalance, weighted AoAs, LOS	Polarization balance, 3D-random AoAs
3. Directive antenna with fixed pointing and polarization:	Realized antenna gain / Deterministic case.	Realized antenna gain & guidelines / Almost det.	Total radiation efficiency & guidelines / Rice.	Total radiation efficiency / Rayleigh.
4. Small non-directive antenna, 3D-random orientation:	Total radiation efficiency / not Rayleigh but can be	Total radiation efficiency / even closer to Rayleigh	Total radiation efficiency / approximately Rayleigh	Total radiation efficiency / Rayleigh
5. Small multiport antenna, 3D-random orientation:	& 1% cumulative LOS-diversity gain in dBR	& 1% cumulative diversity gain in dBR	& 1% cumulative diversity gain in dBR	& 1% cumulative RIMP-diversity gain in dBR

(Left vertical label: **Quality factors of different antennas / Shape of CDF**)
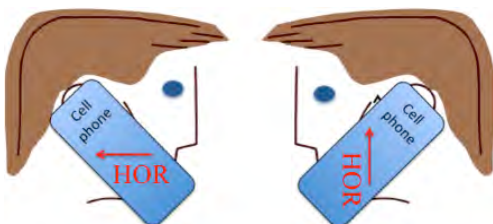
Figure 1.Illustration of the fact that the vertical direction relative to handheld phone-type device is undefined. The red arrow is a marker fixed to the phone by e.g. tape in such a way that it has a horizontal orientation with respect to the environment when the phone is held on the right side of the head. Then, the fixed marker will have a vertical orientation when the same phone is held on the right side of the head.

A. 3D-random LOS due to 3D-random device orientation

The RIMP environment is isotropic, meaning that the statistical properties of the received voltage will not depend on the orientation of the wireless device. We have in line 4 in the table shown the expected performance for small antennas on devices with 3D-random orientations. Most wireless devices will be of this kind, because they do not have any fixed orientation with respect to the vertical axis. This is clear for phone-type devices from the illustration in Figure 1 and explanation in its caption. A related interchanging of horizontal and vertical directions appears in modern hand-held tablets that can be used for any orientation of the screen, i.e., any of its fours edges can be pointing upwards. When considering the 3D-random variation of the orientations of many users including their devices (and hence of the AoA relative to the antenna coordinate system), it is clear that the expectation of the received power must become proportional to the total radiation efficiency, and not the realized gain as in free space LOS environments. Thus, we have effectively a 3D-random LOS.

The CDF of the received voltage is always Rayleigh distributed in RIMP, both for directive and small antennas, but for directive antennas we need a richer RIMP environment for this to be the case than we need for non-directive antennas. On the other hand, the CDF will not necessarily be Rayleigh in 3D-random LOS, but studies [6] have shown that it will be close to Rayleigh provided the antenna is not directive, and provided there are arbitrarily-shaped scattering bodies close to the antenna such as the chassis of the device, the user hand or head. If the polarization of the LOS wave is randomly elliptical, it will also make the CDF more Rayleigh. With

arbitrarily-shaped bodies we mean that the bodies have not been used constructively to optimize the radiation patterns in any way. The more randomness the chassis and user introduce, the more similar is the CDF to the ideal Rayleigh shape. Therefore, we may state that for the real-life environments in columns 2 and 3 in the table, the CDFs will be even closer to Rayleigh than the CDF in column 1 (pure-LOS); valid for the 3D-random orientation cases in lines 4 and 5. *Therefore, we may expect that it is sufficient to evaluate performance of small antennas in the extreme environments pure-LOS and RIMP.*

We will in the next section describe how we can characterize diversity performance in terms of the cumulative diversity gain of the 1% worst users (line 5 in table), and we will use both the two extreme environments pure-LOS and RIMP as examples.

V. CUMULATIVE LOS- AND RIMP-DIVERSITY GAINS OF THE 1% WORST USERS (in dBR relative to Rayleigh)

Diversity and MIMO antennas have multiple ports, and their performance can be quantified by processing the wireless channel between the ports on the transmit side and the ports on the receive side. Previous papers such as [4] have defined the diversity gain from the CDFs in a RIMP environment, by considering a moving user (device). The CDF is generated by collecting time samples of the received channel on each port, as well as of the diversity-combined port. In addition, a CDF is generated from a reference antenna with known efficiency (here assumed to be 100%) in the same RIMP environment. The average received power of the reference CDF is used to normalize the other CDFs. All the single-port CDFs will have shapes identical to a theoretical Rayleigh if the environment is rich enough, which in practice means that the measured CDF should follow the theoretical Rayleigh down to CDF = 1%, corresponding to nearly 10 000 independent samples for good accuracy. However, these single-port CDFs will be shifted to the left relative to the reference CDF by an amount equal to the total embedded radiation efficiency seen at the port.

We illustrate CDFs and diversity-combined CDFs in Figure 2. The CDFs are presented for the cases of: i) RIMP environment as emulated by a reverberation chamber, and ii) 3D-random LOS case. The latter has been obtained from embedded far field functions measured in an anechoic chamber and processed to give the LOS-diversity gains. This processing can be done in a very simple manner for the pure 3D-random pure-LOS case, by sampling the 3D far field functions uniformly over the unit sphere and arranging the samples from lowest to highest levels. We choose here also to simplify the graph by normalizing the CDFs independently for each antenna, to the highest average received power among the two ports. This means that the total embedded radiation efficiencies on the strongest port do not show up in the curves, and that we have to correct for this to compare CDFs and diversity gains of different antennas. This is done in Table 3 by including the total radiation efficiencies in the effective diversity gains, according to the definition in [4]. Figure 2 shows therefore what is referred to as apparent diversity gains

in the same reference.

The apparent RIMP-diversity gain at 1% level is then defined as illustrated in Figure 2: The difference between the 1% levels of the CDF of the diversity-combined signal and the CDF of the ideal Rayleigh curve. The latter is for the present normalization the same as the CDF of the best port of the diversity antenna itself. The definition is the same for the 3D-random LOS-diversity. The values are presented in the "Example, free space" column in Table 3 in dBR, *where dBR means* dB *relative to Rayleigh distribution*.
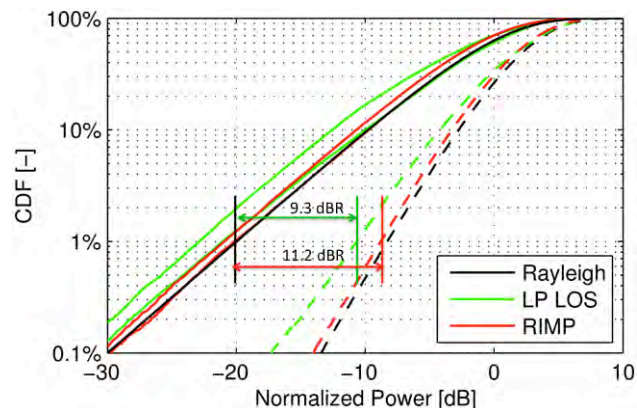
Figure 2. Definitions of apparent cumulative RIMP-diversity gain (11.2 dBR) and LOS-diversity gain (9.3 dBR) of an example of a diversity antenna on a phone-type device in handheld position. The CDFs in the two environments are shown for both ports (solid lines) as well as the CDFs of the MRC cases (dashed lines).. The corresponding ideal Rayleigh cases are also shown. LP LOS means Linearly Polarized LOS.

Table 3. Cumulative RIMP- and LOS-diversity gains of two orthogonal small dipoles, and practical example of 2-port diversity antenna at 2.2 GHz. The example antenna is located on a mock-up of a mobile phone that has two locations: free space and handheld. [1]The LOS-diversity gain is for linearly polarized 3D-random LOS. [2]The value -0.2 dBR on the reference port deviate from the true value of 0.0 dBR due to numerical uncertainty, and the value on the second port is lower due to a power imbalance between the two.

Antenna type	2 small dipoles	Example, free space	Example, handheld
Total embedded element efficiency, ports 1 & 2	0 dB	-0.8 & -1.5 dB	-3.0 & -4.5 dB
1% LP LOS CDF level	-14.8 dBR	-1. & -.9 dBR	-1.1 & -2.9 dBR
LOS-diversity gain	7.1 dBR	9.3 dBR	9.3 dBR
Effective LOS-diversity gain	**7.1 dBR**	**8.5 dBR**	**6.0 dBR**
1% RIMP CDF level	0 dBR	-.5 dBR	-0.2 & -1.0 dBR[2]
RIMP-diversity gain[1]	11.7 dBR	11.1 dBR	11.2 dBR
Effective RIMP-diversity gain	**11.7 dBR**	**10.3 dBR**	**8.2 dBR**

The shapes of the RIMP-CDFs will converge very slowly at 1% level, and therefore it is advantageous to use techniques by which we can compute diversity gain already after 100 independent samples [13, 14]. These algorithms are very useful independent of how the channel is generated. In principle they are based on first determining the average

power received on each port and the correlation between the signals on the two ports, all of which converges well after 100 samples, and then plugging these values into a formula valid for Rayleigh distributions. This approach cannot be used for 3D-random LOS-diversity gain, unless we are completely sure that the CDFs have Rayleigh shape.

Table 3 shows also theoretical results for two orthogonal small dipoles. We see that they have very low 1% LOS-CDF level (-14.8 dBR) so their LOS-CDFs are very far from Rayleigh shape and the performance very bad, whereas the example antenna is very close to Rayleigh. The RIMP-CDFs are almost equal to Rayleigh like they should be, except for a shift on one port due to different radiation efficiencies on the two ports. Two orthogonal dipoles are better (7.1 dBR), but still worse than the practical example with LOS-diversity gain of 9.3 dBR.

The example device used for the illustration above is a mock-up of a mobile phone of size 115 mm × 55 mm × 12 mm with the antennas located along the two 55 mm sides, and it was measured at 33 frequency points in each of the frequency bands 750 – 960 MHz and 1700 – 2700 MHz. Some results are presented in [6]. The results selected for Figure 2 and Table 3 are quite representative, even though these do not show the spreads of the LOS CDF levels and LOS-diversity gains over the two frequency bands, which was up to 7 dB for the four different cases (low band & high band for free space & handheld). There are in [6] also shown results for theoretical Huygens sources, and for circularly polarized LOS.

Previously the 1% diversity gain was interpreted as the gain for a single moving user in his 1% worst situations. Now, when we use CDFs representing the distribution of performance among several users, we must interpret it as the cumulative improvement for the 1% users with the worst receiving conditions. The cumulative user-distributed RIMP-diversity gain is identical to the previous single-user gain during fading. However, the *3D-random LOS-diversity gain can only be interpreted as a cumulative improvement for the 1% worst users*, because the CDFs are created for 3D-random orientations only being representative for a distribution of users.

We will now describe how the reverberation chamber can be used to emulate a RIMP environment with different time delay spreads.

VI. THE REVERBERATION CHAMBER

The reverberation chamber was already 20 years ago [9] known to create Rayleigh fading when the modes were stirred by mechanical movement of plates or shaped wires (mechanical stirrers). In [21] it was shown that the modes represent plane waves with an omni-directional distribution of AoA, provided the chamber is large enough. Thus, the reverberation chamber corresponds to RIMP environment. The stirring techniques were improved in order to ensure emulation of a rich enough RIMP environment to accurately measure efficiency-related quantities such as radiation efficiency, radiated power and receiver sensitivity. These techniques included platform stirring and polarization stirring,

see the overview of all developments described in [22]. Platform stirring is important to get sufficient accuracy for OTA measurements.

There has been performed direct comparisons of the statistical field characteristics of real-life environments and in reverberation chambers, showing good agreement [23].

B. Hill's average power transfer formula and the descriptive average mode bandwidth

The principle of operation of the reverberation chamber is based on Hill's formula for the average power transfer function between two antennas located in a reverberation chamber [8], i.e.

$$G_{chamber} = \frac{P_r}{P_t} = \frac{1}{N}\sum_{n=1}^{N}\left|H_{t,r,n}\right|^2 = \frac{c^3 e_{rad,t} e_{rad,r}}{16\pi^2 V f^2 \Delta f} \qquad (1)$$

where P_t is the maximum available transmit power (for transmitting antenna matched for radiation into free space), and P_r is average received power at the port of the receiving antenna. The averaging must be done over sufficiently number of independent samples N of the complex channel $H_{t,r,n}$ between the ports of the two antennas when the stirrers are moved, with the movement given by changes in the index n. $H_{t,r,n}$ is actually the complex S-parameter of the reverberation chamber as measured with a standard vector network analyzer (VNA). In Hill´s formula f is the frequency, c is velocity of light, V is the chamber volume, $e_{totrad1}$ and $e_{totrad2}$ are the total radiation efficiencies of the two antennas including the impedance mismatch factors for free space case, and Δf is the average mode bandwidth. Thus, in the average power transfer function the free space mismatch factors come in, because the effect of the chamber on the mismatch is statistical with zero mean. The average mode bandwidth Δf consists of four additive contributions due to wall losses, leakage from slots, antennas in the chamber, and absorbing objects [8, 15].
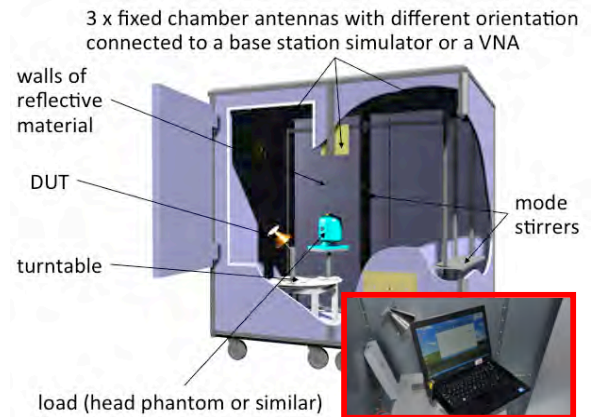
Figure 3. *Drawing of interior of reverberation chamber for OTA measurements. The inserted photo shows the case of a laptop with a USB-type LTE modem located inside the chamber for throughput measurements. The DUT is in this case a wideband calibration antenna, seen also on photo.*

Hill's original formula included the Q-factor $Q = f/\Delta f$ instead of the average mode bandwidth Δf. However, by replacing Q by Δf, the formula becomes clearer because then the dominant frequency variation of $G_{chamber}$ is given by the

explicit $1/f^2$ factor. It has turned out that for practical reverberation chambers for OTA measurements Δf is almost constant with frequency, so that the value of Δf describes the chamber very well over a large frequency range. Further, Δf is identical to the coherence bandwidth of the statistical multipath emulated by the chamber [16]. Finally, Δf is proportional to the average K-factor [24], and thereby the resulting increased uncertainty can be estimated [15]. Thus, Δf is a very important quantity when characterizing reverberation chambers.

It is evident from Hill's formula that the reverberation chamber can be used to measure efficiency related quantities. First, we measure a reference case, i.e. the average reference received power P_{ref} by using a reference antenna with known total radiation efficiency e_{ref}. Thereafter, we measure the average received power P_{AUT} of the antenna under test (AUT), and finally the total radiation efficiency of the AUT can be determined as

$$e_{AUT} = e_{ref} \frac{P_{AUT}}{P_{ref}} \qquad (2)$$

B. Uncertainty and coherence bandwidth

The accuracy of the measurements improves with the number of modes that are excited, i.e. with the mode density, and therefore with the size of the chamber in wavelengths. This means that there exists a certain lowest frequency of operation, above which the uncertainty is better than a given limit. The chamber used in the present study has an uncertainty better than 0.3 dB RMS above 650 MHz. The uncertainty has through the years been carefully validated by comparison with measurements in anechoic chambers and larger reverberation chambers, see [22] for the references.

The uncertainty was recently studied in more detail, because the uncertainty did not improve with frequency as it should according to [9] and the increasing mode density. The reason was found to be a LOS-type contribution to the wireless channel through the chamber [15], and it was found that this could be characterized by an average Rician K-factor [24]. This acknowledgement motivated a redesign of the chamber, involving removing the fixed wall antennas from the walls of the chamber and relocating them orthogonal to each other on a support tower behind a cornered shield. Thereby, the direct LOS was removed and the K-factor was significantly reduced, and this improved the uncertainty to 0.3 dB RMS from 650 MHz and upwards for the chamber shown in Figure 3, which has a size of 1.8 m × 1.7 m × 1.2 m [15]. This measurement uncertainty is very competitive to what can be achieved from good anechoic chamber, and the present reverberation chambers have always been performing well on round robin tests of radiation efficiency, radiated power and receiver sensitivity.

Coherence bandwidth will increase when the chamber is loaded with lossy objects. Then, the average mode bandwidth Δf increases, and the average power transfer function decreases according to Hills formula. However, the LOS component will not be affected and will therefore effectively increase relative to the average power transfer function given by Hill's formula, so the measurement uncertainty gets worse, but the uncertainty will still stay within acceptable limits if the loading is moderate [15]. We normally use the chamber with some loading inside it, such as e.g. a head phantom. We have also studied the effect of additional loads in the form of PVC cylinders filled with microwave absorbers and located along orthogonal inner corners of the chamber, as described in [16] and defined by Table 4. The extents of coherence bandwidths and time delay spreads that were achieved are summarized in Table 4 together with the STD uncertainties. The RMS time delay spreads are within the ranges appearing in real-life environments.

Table 4. Approximate coherence bandwidths, RMS time delay spreads and measurement uncertainty (STD) for different loadings of the reverberation chamber in Figure 3 over the frequency range 1.2 – 2.7 GHz. The extra loads are PVC cylinders filled with microwave absorbers.

Load	Coherence bandwidth	RMS delay spread	STD w/ platform	STD, no platform
Empty	1 - 2 MHz	220-150 ns	< 0.2 dB	<0.4 dB
Head phantom	3 - 3 MHz	100-130 ns	< 0.3 dB	< 1 dB
+3 extra loads	7 MHz	40 ns	< 0.5 dB	< 1.5 dB
+ 6 extra loads	10 MHz	30-25 ns	-	-

VII. CHARACTERIZATION OF ACTIVE WIRELESS DEVICES

It is straight forward to measure total radiated power in the reverberation chamber, and it has been shown in several papers that bit error rates (BER) also can be measured if the chamber is appropriately loaded so that the coherence bandwidth becomes similar to the real-life environment we want to emulate [25, 26]. We here briefly describe how these measurements are done, and we will in Section VIII extend the latter BER measurements to data throughput measurements, and present a simple good theoretical model for the same.
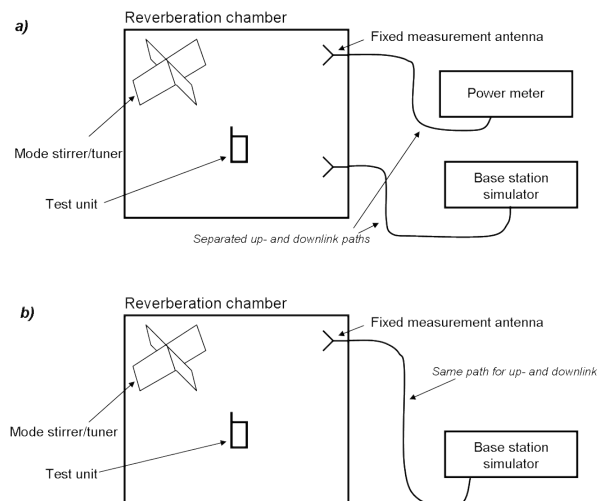
Figure 4. Two schematic setups for measuring TRP. Alternative b can also be used for measuring receiver sensitivity and throughput.

C. Measuring Total Radiated Power (TRP)

For active device under test (DUT), the TRP is determined by the power output from the amplifier and the radiation efficiency of the antenna. TRP is therefore often used as a performance parameter. The TRP measurement procedure is similar to the radiation efficiency procedure described

between equations (1) and (2), with the main difference that we have replaced the VNA with a base station simulator and power meter as shown in Figure 4. The base station simulator is used to establish and maintain a connection to the DUT and control its traffic channel and output power. The power meter is used to sample the transmitted power, and could be a spectrum analyzer, base station emulator with integrated power meter, or a regular power meter, whichever is available.

D. Measuring static receiver sensitivity

The receiver sensitivity will appear differently in a static environment with a stationary user (no fading) and in the dynamic case with time-varying fading. For the static case the antenna performance must also be taken correctly into account, and this is done via the standardized approaches for measuring Total Isotropic Sensitivity (TIS) and Total Radiated Sensitivity (TRS) in anechoic chambers. These two similar approaches are standardized by the CTIA and 3GPP organizations, respectively. The TIS sensitivity is specified at a certain bit error rate (BER, used in GSM and WCDMA), or related frame error rate (FER, used in CDMA2000) or block error rate (BLER, used in HSPA) for the more advanced communication systems. We will here instead of FER and BLER use the joint term Group Error Rate (GER) in order to cover them all.

TIS can also be measured in a reverberation chamber, but then by determining the sensitivity values at several stirrer positions n, each time under static stirring conditions, and averaging these values, according to

$$TIS = \left(\frac{1}{N} \sum_{n=1}^{N} \frac{G_{chamber}}{P_{BSS,n}} \right)^{-1} \qquad (3)$$

where $P_{BSS,n}$ is the reading of the power from the base station simulator at each stirrer position, and $G_{chamber}$ is the average power transfer function of the chamber in (1) achieved from the chamber calibration. Note that $G_{chamber}$ is constant in (3), and could have been taken outside the summation sign.

Simply explained, the TIS parameter is equal to the sensitivity of the DUT as measured by a connected cable, degraded by the radiation efficiency of the antenna.

E. Measuring average receiver sensitivity during fading

The ultimate performance metric for the receiving case is the average sensitivity during fading, i.e. the GER during fading. This shows large improvements when diversity and MIMO algorithms are used. This realistic dynamic sensitivity approach has been implemented for measurements in the reverberation chamber, during continuous movements of the stirrers, referred to as average fading sensitivity (AFS) [11]. It is worth noticing that when the fading is frequency-flat, the TIS can be derived from the AFS value since there is a theoretical relation between the two values. This relation is given by the following formula between the static GER and the average GER in the dynamic case, i.e

$$GER_{av}(P_{av}) = \int_{-\infty}^{\infty} GER_{static}(P) \, PDF(P / P_{av}) \, dP \qquad (4)$$

where $PDF(P/P_{av})$ is the probability distribution of the fading

power P at the receiver input, and P_{av} is the average value of P over a fading cycle, i.e. taken over the complete stirring sequence. For Rayleigh fading this PDF is the exponential distribution. The averaging integral is taken over all levels of P during the fading.

Throughput data rate in systems with MIMO and OFDM is measured with the same setup as for measuring AFS.

VIII. Modeling Measured Throughput for System with MIMO and OFDM Frequency Diversity

A. Ideal threshold receiver

It is well known that FER and BLER curves, i.e. GER curves, are much steeper than BER curves when presented as a function of instantaneous received power, i.e., the GER decreases very suddenly from 1 (only errors) to zero (no errors) when the received power level increases above a certain threshold, whereas the BER curves in the first wireless systems approached zero much more slowly. The solid vertical curve in Figure 5 shows the measured throughput (i.e. 1 - GER) of a typical LTE device when we connect a cable to its antenna port, and we can see that it increases from 10% to 90 % when the signal power increases by 0.4 dB. However, it is important to be aware that the threshold varies with modulation, as well as MIMO configuration in advanced receivers. The reason for this difference between BER and GER is that the latter make use of blocks or frames of bits including bits that correct for bit errors by using so-called forward error correction codes, and the receiver is able to correct for the errors caused by white Gaussian noise when the channel power decreases, but only to a certain limit when the reception suddenly brakes down.

We have in [12] used this characteristic of GER to define an ideal error correction receiver for convenience and simplicity, by

$$GER_{ideal}(P) = \begin{cases} 1 & \text{when } P < P_{th} \\ 0 & \text{when } P > P_{th} \end{cases} \qquad (5)$$

where P_{th} is the threshold level, which in Figure 5 is –83.7 dBm (corresponding to the 50% throughput value for the conducted case). The relative instantaneous throughput data rate can for such case simply be written as

$$Tput = Maxrate * \{1 - GER(P)\} \qquad (6)$$

where $Maxrate$ is the data rate set by the system.

B. Average throughput during fading

The formula for the average GER during fading becomes in particular simple for this ideal threshold receiver. By combining (4) and (5), and then using (6) we get

$$GER_{av}(P_{av}) = \int_{-\infty}^{P_{c}} PDF(P / P_{av}) dP = CDF(P_{th} / P_{av}) \qquad (7)$$

$$Tput(P_{av}) = Maxrate * \{1 - CDF(P_{th} / P_{av})\}$$

where CDF is the cumulative distribution function of the fading channel power distribution. We see that for the ideal threshold receiver the relative throughput data rate is equal to 1- CDF of the power distribution of the fading signal at the

threshold level.

The measurement setup for throughput data rate shown in Figure 4 was used to test a commercial USB modem provided with external antennas [12]. The RMS delay spread of the reverberation chamber was tuned in to 90 ns corresponding to a coherence bandwidth of 3 MHz. The measurements was done in the LTE band 7, channel 2850 (2630 MHz) with 10 MHz total channel bandwidth. The fixed data rate from the base station was 64QAM, i.e. 24 Mbps for 2×1 MISO diversity system.

The measured throughput results are presented in Figure 5 together with theoretical curves obtained by using (7). The theoretical model is given by (7) with the measured P_{th} = -83.7 dBm. The CDFs were obtained by numerically generating Rayleigh distributions with average power equal to unity, and then combining these using MRC, assuming no correlation between the channels. The 1×1 SISO case represents one such Rayleigh CDF. The 1×2 SIMO makes use of two uncorrelated CDFs and MRC-combines them without averaging the power, thereby giving 3 dB power gain. We show one additional theoretical curve where we have MRC-combined N_{fd}=2 uncorrelated frequency channels according to simple OFDM algorithm with power averaging so there is no power gain. We see that the agreement with the measurements is very good both regarding location along the power axis and slope. The first is a result of very good calibration of the average power transfer function of the chamber, the cables connecting the instrument and the USB device to the chamber, and the cables connecting these to each other during the measurements of the receiver threshold, and of the mismatch factor of the external antennas connected to the device. The agreement between the slopes of the measured and theoretical curves means that the diversity order of the theoretical model is correct. We can explain this from the RMS delay spread which was 90 ns, corresponding to 3 MHz coherence bandwidth (Table 4). This evidently means that we cannot get more than 1 diversity order out of the implemented OFDM algorithm in the device for 90 ns RMS time delay spread. We also loaded the chamber more to achieve 9 MHz coherence bandwidth. Then, the slope of the throughput curve (not shown) changed to agree with a theoretical curve with no frequency diversity, i.e. N_{fd}=1. Some more results included correlated antennas can be found in [12], and a more thorough study of OFDM diversity effects for more time delay spreads (chamber loadings) are ongoing.

C. Shannon's Maximum Available Capacity

The maximum available MIMO capacity can be computed from the channel matrix by using the theoretical extended Shannon formula as explained in [10, 27]. Such results can be presented as a function of signal to noise ratio, and represents a theoretical maximum which is almost impossible to achieve in practice. Unfortunately, such curves do not resemble measured throughput curves at all. However, the theoretical Shannon capacity is a measure of the quality of the throughput curve at its knee, i.e. where the throughput curve almost has reached its maximum. Therefore, it makes sense to perform studies of the Shannon capacity using theoretical or measured

channel matrices including the antenna. It is important that the modeling is done by using embedded far field functions on the ports of the MIMO antenna Then, such capacity results will show good agreement with results based on measured channels in reverberation chamber [4, 10]. The agreement is also good if the embedded far field functions are measured in an anechoic chamber, as documented in [27] by measuring a wideband multiport antenna over the bandwidth 2 – 8 GHz. We will not show such results here in the present paper.
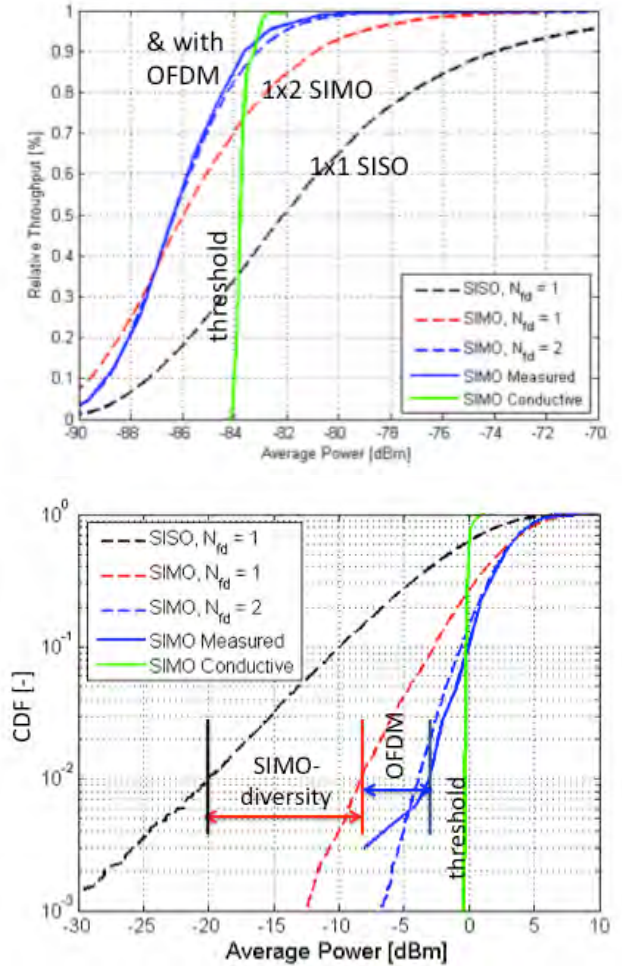
Figure 5. Theoretical (dashed) and measured (solid) results for throughput (upper) and corresponding CDFs using (8), for LTE device with 2-port MIMO antennas. The vertical line is the threshold line of the digital receiver measured with a cable connected to the antenna port. The threshold value used to produce theoretical curves is -83.7 dBm.

IX. USING THROUGHPUT CURVES TO DETERMINE CUMULATIVE PERFORMANCE OF 1% WORST USERS

The CDFs of the channel function can be determined from the measured throughput in (7). This is interesting, because it becomes easier to interpret the details of the throughput and GER curves. The lower graph in Figure 5 shows the CDFs corresponding to all the throughput curves in the upper graph. Here we can see the effects of the SIMO 1×2 diversity as well as the OFDM diversity very clearly, and we can of course also relate it to the cumulative CDF over randomly distributed

users and devices in the RIMP environment, as discussed in Section V. Thus, throughput curves give us information about the user-distributed performance of the system, but this is more easy to quantify by plotting CDF curves with a logarithmic vertical axis. For our example, the SIMO diversity is seen to represent a RIMP-diversity gain of 12 dB, and the OFDM give an additional 5 dB RIMP-diversity gain, both according to Figure 5.

X. CONCLUSIONS

We have described different wireless communication environments, in which the statistics of user locations and device orientations are taken into consideration in the determination of the characteristics of the channel. Then, it is clear that there will never be any fixed LOS, but rather a random LOS, because we have to study the distributions of the orientations of the users and their wireless devices in order to make decisions about the quality of a wireless device for use in multipath environments.

We have described the RIMP (rich isotropic multipath) environment as a new and extreme reference environment for characterizing antennas and wireless devices for use in multipath. This complements the classical opposite extreme anechoic pure-LOS environment. The RIMP environment can be emulated in a reverberation chamber, and the anechoic chamber is traditionally used to emulate pure-LOS.

We have introduced a new interpretation of the RIMP-diversity gain, by letting it represent also the cumulative performance improvement of the 1% worst users in the environment. And, we have developed a related but not necessarily equal LOS-diversity gain for pure-LOS environment. To determine the latter we need to know the embedded far field functions on the MIMO antenna ports. We expect that both these two diversity gains are sufficient to distinguish good and bad wireless devices, and thereby to ensure good performance also in real-life environments that are somewhere in between the two extreme pure-LOS and RIMP environments.

We have explained the procedures for measuring total radiated power and receiver sensitivity of active devices in reverberation chamber. These have lately been complemented with measurements of throughput data rate of complete wireless devices. The measured results are repeatable under similar conditions, but at different locations and orientations in the reverberation chamber. In order to understand the measured throughput results we have developed a simple theoretical model. This is based on a simple threshold receiver model. This ideal threshold receiver makes it possible to determine the throughput data rate directly from the CDF of the MIMO diversity combined signal statistics, and visa versa. The threshold model has proven to be able to predict the shape and absolute values of measured throughput curves versus maximum available received power in LTE systems, including the effect of the MIMO diversity as well as the OFDM frequency diversity under frequency-selective fading conditions.

There are still challenges in developing the reverberation chamber technology further. E.g., there are large opportunities in using two connected reverberation chambers for more advanced system tests (one chamber for each side of the communication system), and, connecting an anechoic chamber (with a "mast-located" base station) and a reverberation chamber (with the device) together. Some initial tests of connected reverberation chambers were demonstrated in [28], and these test could detect exciting propagation phenomena like key-hole effects which previously was observed and studied in theoretical propagation research [29].

XI. ACKNOWLEDGMENTS

REFERENCES

[1] G. Alfano and A. De Maio, "Sum of Squared Shadowed-Rice Random Variables and its Application to Communication Systems Performance Prediction," *Wireless Communications, IEEE Transactions on,* vol. 6, pp. 3540-3545, 2007.

[2] M. Godavarti, T. L. Marzetta, and S. Shamai, "Capacity of a mobile multiple-antenna wireless link with isotropically random Rician fading," *Information Theory, IEEE Transactions on,* vol. 49, pp. 3330-3334, 2003.

[3] A. Sibille and M. A. Mellah, "A statistical model of handsets effective gain accounting for user influence and local propagation," in *Antennas and Propagation (EuCAP), 2010 Proceedings of the Fourth European Conference on,* 2010, pp. 1-4.

[4] P. S. Kildal and K. Rosengren, "Correlation and capacity of MIMO systems and mutual coupling, radiation efficiency, and diversity gain of their antennas: simulations and measurements in a reverberation chamber," *Communications Magazine, IEEE,* vol. 42, pp. 104-112, 2004.

[5] P. S. Kildal and K. Rosengren, "Electromagnetic analysis of effective and apparent diversity gain of two parallel dipoles," *Antennas and Wireless Propagation Letters, IEEE,* vol. 2, pp. 9-13, 2003.

[6] P.-S. Kildal, U. Carlberg, and J. Carlsson, "Definition of Antenna Diversity Gain in User-Distributed 3D-Random Line-Of-Sight," *submitted to IEEE Antennas and Wireless Propagation Letters (AWPL),* September 2011.

[7] M. L. Bäckström, O.; Kildal, P. S., "Reverberation chambers for EMC susceptibility and emission analyses," *Review of Radio Science,* pp. 429-452, 1999.

[8] D. A. Hill, M. T. Ma, A. R. Ondrejka, B. F. Riddle, M. L. Crawford, and R. T. Johnk, "Aperture excitation of electrically large, lossy cavities," *Electromagnetic Compatibility, IEEE Transactions on,* vol. 36, pp. 169-178, 1994.

[9] J. G. Kostas and B. Boverie, "Statistical model for a mode-stirred chamber," *Electromagnetic Compatibility, IEEE Transactions on,* vol. 33, pp. 366-370, 1991.

[10] K. Rosengren and P. S. Kildal, "Radiation efficiency, correlation, diversity gain and capacity of a six-monopole antenna array for a MIMO system: theory, simulation and measurement in reverberation chamber," *Microwaves, Antennas and Propagation, IEE Proceedings -,* vol. 152, pp. 7-16, 2005.

[11] C. Orlenius, P. S. Kildal, and G. Poilasne, "Measurements of total isotropic sensitivity and average fading sensitivity of CDMA phones in reverberation chamber," *2005 IEEE Antennas and Propagation Society International Symposium, 3-8 July 2005,* vol. Vol. 1A, pp. 409-12, 2005.

[12] P. S. Kildal, A. Hussain, X. Chen, C. Orlenius, A. Skårbratt, J. Åsberg, T. Svensson, and T. Eriksson, "Threshold Receiver Model for Throughput of Wireless Devices with MIMO and Frequency Diversity Measured in Reverberation Chamber," *IEEE Antennas and Propagation Wireless Letters,* vol. 10, pp. 1201-1204, October 2011.

[13] N. Jamaly, P. S. Kildal, and J. Carlsson, "Compact Formulas for Diversity Gain of Two-Port Antennas," *Antennas and Wireless Propagation Letters, IEEE,* vol. 9, pp. 970-973, 2010.

[14] X. Chen, P. S. Kildal, and J. Carlsson, "Fast converging measurement of MRC diversity gain in reverberation chamber using covariance-eigenvalue approach," *IEICE Transactions on Electronics,* vol. E94-C, pp. 1657-1660, Oct. 2011.

[15] P.-S. Kildal, X. Chen, C. Orlenius, M. Franzén, and C. Lötbäck Patané, "Characterization of Reverberation Chambers for OTA Measurements of Wireless Devices: Formulation of Channel Matrix and Uncertainty," *submitted to IEEE Transactions on Antennas and Propagation,* September 2011.

[16] X. Chen, P. S. Kildal, C. Orlenius, and J. Carlsson, "Channel Sounding of Loaded Reverberation Chamber for Over-the-Air Testing of Wireless Devices: Coherence Bandwidth Versus Average Mode Bandwidth and Delay Spread," *Antennas and Wireless Propagation Letters, IEEE,* vol. 8, pp. 678-681, 2009.

[17] P. O. Iversen, P. Garreau, and D. Burrell, "Real-time spherical near-field handset antenna measurements," *Antennas and Propagation Magazine, IEEE,* vol. 43, pp. 90-94, 2001.

[18] P. Hallbjörner, Z. Ying, M. Håkansson, C. Wingqvist, T. Anttila, and J. Welinder, "Multipath simulator for mobile terminal antenna characterisation," *Microwaves, Antennas & Propagation, IET,* vol. 4, pp. 743-750, 2010.

[19] A. Yamamoto, T. Sakata, T. Hayashi, K. Ogawa, J. O. Nielsen, G. F. Pedersen, J. Takada, and K. Sakaguchi, "Effectiveness of a fading emulator in evaluating the performance of MIMO systems by comparison with a propagation test," in *Antennas and Propagation (EuCAP), 2010 Proceedings of the Fourth European Conference on*, 2010, pp. 1-5.

[20] A. Goldsmith, *Wireless Communications*: Cambridge University Press, 2005.

[21] K. Rosengren and P. S. Kildal, "Study of distributions of modes and plane waves in reverberation chambers for the characterization of antennas in a multipath environment," *Microwave and Optical Technology Letters,* vol. 30, pp. 386-91, 2001.

[22] P. S. Kildal, C. Orlenius, J. Carlsson, U. Carlberg, K. Karlsson, and M. Franzen, "Designing reverberation chambers for measurements of small antennas and wireless terminals: Accuracy, frequency resolution, lowest frequency of operation, loading and shielding of chamber," in *Antennas and Propagation, 2006. EuCAP 2006. First European Conference on*, 2006, pp. 1-6.

[23] H. Fielitz, K. A. Remley, C. L. Holloway, Z. Qian, W. Qiong, and D. W. Matolak, "Reverberation-Chamber Test Environment for Outdoor Urban Wireless Propagation Studies," *Antennas and Wireless Propagation Letters, IEEE,* vol. 9, pp. 52-56, 2010.

[24] X. Chen, P. S. Kildal, and S. H. Lai, "Estimation of Average Rician K-Factor and Average Mode Bandwidth in Loaded Reverberation Chamber," *Antennas and Wireless Propagation Letters, IEEE,* vol. 10, pp. 1437-1440, 2011.

[25] E. Genender, C. L. Holloway, K. A. Remley, J. M. Ladbury, G. Koepke, and H. Garbe, "Simulating the Multipath Channel With a Reverberation Chamber: Application to Bit Error Rate Measurements," *Electromagnetic Compatibility, IEEE Transactions on,* vol. 52, pp. 766-777, 2010.

[26] S. J. Floris, K. A. Remley, and C. L. Holloway, "Bit Error Rate Measurements in Reverberation Chambers Using Real-Time Vector Receivers," *Antennas and Wireless Propagation Letters, IEEE,* vol. 9, pp. 619-622, 2010.

[27] X. Chen, P. S. Kildal, J. Carlsson, and J. Yang, "Comparison of Ergodic Capacities From Wideband MIMO Antenna Measurements in Reverberation Chamber and Anechoic Chamber," *Antennas and Wireless Propagation Letters, IEEE,* vol. 10, pp. 446-449, 2011.

[28] C. Orlenius and M. Andersson, "Repeatable performance measurements of MIMO systems in connected reverberation chambers with controlled keyhole effect," in *Antennas and Propagation, 2009. EuCAP 2009. 3rd European Conference on*, 2009, pp. 1086-1089.

[29] D. Chizhik, G. Foschini, M. Gans, and R. Valenzuela, "Key-holes, correlations, and capacities of multielement transmit and receive antennas," *IEEE Trans. Wireless Commun.,* vol. 1, pp. 361-368, Apr. 2002.

Per-Simon Kildal (M'76–SM'81–F'95) is professor in antennas at Chalmers University of Technology in Gothenburg, Sweden since 1989. He is heading the Antenna group. His main tasks are to lead and supervise research and education within antenna systems. 18 persons has received Ph.D. from him.

Kildal has authored more than 120 articles in scientific journals; concerning antenna theory, analysis, design and measurements, two of which was awarded best paper awards by IEEE (1985 R.W.P. King Award and 1991 Schelkunoff Prize Paper Award). In 2011 he was awarded the prestigious Distinguished Achievements Award from the IEEE Antennas and Propagation Society.

Kildal has done the electrical design of the 40m x 120 m cylindrical reflector antenna and line feed of the EISCAT scientific organization, and the dual-reflector Gregorian feed of the 300 m Ø radio telescope in Arecibo. He is the inventor behind technologies such as dipole with beam forming ring, the hat antenna, and the eleven feed. Kildal was the first to introduce the reverberation chamber as an accurate measurement instrument tool for Over-The-Air (OTA) characterization of small antennas and wireless terminals for use in multipath environments with fading. Kildal is also the originator of the concept of soft and hard surfaces from 1988, today being regarded as the first metamaterials concept. This concept is the basis of his newest and most fundamental invention, the gap waveguide technology. His research is innovative and industrially oriented, and has resulted in several patents and related spinoff companies, the most known being Bluetest AB.

Kildal organizes and lectures in courses within the *European School of Antenna* (ESoA, www.antennasvce.org). His textbook *Foundations of Antennas - A Unified Approach* (Lund, Sweden: Studentlitteratur, 2000) was well received, and is now in the process of being revised.

Charlie Orlenius (M'10) was born in Vrigstad, Sweden, in 1976. He received the Master of Science degree in Engineering Physics from Chalmers University of Technology, Gothenburg, Sweden, in 2001. Since 2001, he has been with Bluetest AB, Gothenburg, Sweden, working with research and development of reverberation chambers for testing of small antennas and wireless units. Currently he holds the position of Chief Technology Officer at Bluetest. He is also with the Antenna Group, Department of Signals and Systems, Chalmers University of Technology, participating in the research activities regarding reverberation chambers. He is the author and coauthor of a large number of papers, book chapters and conference contributions about measurements in reverberation chamber.

Jan Carlsson (M'98) was born in Sweden on May 6, 1962. He received the M.S.E.E. and Ph.D. degrees from Chalmers University of Technology, Gothenburg, Sweden, in 1986 and 1998, respectively. From 1986 to 1990, he was an Electromagnetic Compatibility (EMC) Engineer with Ericsson Radar Electronics AB, Mölndal, Sweden. He is currently the Head of Research in the EMC Department, SP Technical Research Institute of Sweden, Borås, Sweden. He is also an Adjunct Professor of computational electromagnetics in the Department of Signals and Systems, Chalmers University of Technology. His current research interests include the area of computation techniques for electromagnetic problems, especially for applications in EMC and antennas. Since 2009 he is assistant centre manager of Chase, Chalmers Antenna Systems VINN EXcellence Centre at Chalmers University of Technology. He is the coauthor of the *EMMA Handbook* (EMC handbook issued by the Swedish Defence Materiel Administration). Dr. Carlsson has been a reviewer for several international journals. From 2002-2004 he was the Chairman of the Swedish IEEE EMC Chapter. Dr. Carlsson is a Member of the Swedish National Committee for Radio Science (SNRV), Section E.